Geology, Geophysics & Environment 2025, vol. 51 (2): 149–172

Local tectonic stress regime in the Upper Silesian Coal Basin using primary geodetic data

Zbigniew Szczerbowski

AGH University of Krakow, Faculty of Geo-Data Science, Geodesy, and Environmental Engineering, Krakow, Poland, email: szczerbo@agh.edu.pl, ORCID ID: 0000-0002-2398-559X

Received: December 30, 2024; accepted: May 11, 2025; first published online: June 25, 2025

Abstract: Many papers have been devoted to the problematic tectonic stress regime of the Upper Silesian Coal Basin (USCB), particularly relating to the interrelation between the tremors triggered by mining activity and the natural seismicity in the rock mass. This problem is analysed here on the basis of geodetic data in light of the tectonic setting. The author determined the horizontal strain regime in the USCB area with the application of triangular arrays that are formed by a network of GPS/GNSS stations. The primary geodetic data used in this research are the coordinates recorded in time by the stations. They enabled the calculation of the easting and northing components of displacement velocity vector and their errors. 16 permanently installed GPS/GNSS stations are located into the study area and this set led to the construction of 23 different triangles, while the centroid of each triangle was extracted. For each centroid, the deformation parameters were determined: maximal horizontal extension, azimuth of maximal horizontal extension, minimal horizontal extension, maximal shear strain, and area strain. These results were applied to estimate the spatial distributions of the parameters. The distributions reveal that the central part of the study area (the Upper Silesian Trough) is under compression, and is surrounded by extension zones. In general, the distributions of strain estimates correspond to the tectonic pattern of the area. These findings provide a different perspective on former studies on tectonic stress by geological surveys and tectonic influence on seismicity in the USCB area. They confirm earlier assumptions about the occurrence of tectonic stress in the studied area. The determined deformation parameters and their spatial distribution provide an explanation for the occurrence of high-energy tremors in the USCB area.

Keywords: Global Navigation Satellite System (GNSS), tectonic regime, triangulation method, geodetic strain, strain parameters

INTRODUCTION

The mining operations carried out for 200 years in the Upper Silesian Coal Basin (USCB), have caused disturbances in the distribution of the rock mass stress and tension. One consequence of the process of this stress accumulation has been the occurrence of seismic tremors. The geological setting of the USCB has been under discussion for a number of years. Many papers have been devoted to the problematic tectonic stress regime, particularly relating to the interrelation between the tremors triggered by the mining and the natural seismicity in the rock mass (e.g., Teisseyre 1983, Gibowicz 1990, Zuberek 1993, Idziak et al. 1999, Patyńska & Stec 2017). Some tectonic aspects of the study area are still a matter of debate, especially with regard to the relationships between the tectonics and the seismic activity of the Upper Silesian Coal Basin. Some research in the area suggests that generating the strongest events have had a strict connection with the tectonics.

https://doi.org/10.7494/geol.2025.51.2.149 ISSN 2299-8004 | e-ISSN 2353-0790 | Wydawnictwa AGH

The tremors with the largest energy have been closely related to geological discontinuities in the area and are regarded as being the results of unstable movements in major geological faults due to the approaching of mining activity (Teper et al. 1992). One example of this problem (which will be discussed later in the paper) is the Kłodnica Fault zone (the central part of the area), which is considered by some authors to be a modern seismogenic structure where The Young-Alpine tectonic stresses have had a significant impact on the nature of mining-induced tremors (Teper & Sagan 1995, Jura 1999). Although there are significant faults in the area under study, their impact on the earth's surface in terms of displacements has not yet been documented.

Geodetic data, despite the significant advances in geodesy that have been made in recent years, are still relatively underused in the structural geology community. The author of this research has undertaken a study on the geodetic strain rates determining them by GPS/GNSS measurements carried out over years in the area. So, basing these results on the time series depicting changes of the positions of the GPS/GNSS stations, strain parameters were evaluated. The geodetic characteristics were compared with the geological data in order to arrive at an evaluation of the manifestation of the tectonic stress on the terrain surface. The presented GPS/GNSS data are dense enough to consider the continuous nature of the surface deformation in the area and are the results of long-time observations. The problem of the influence of non-tectonic factors on the measurement data is also discussed.

In this study, the horizontal strain regime in triangular arrays that are formed by a network of GPS/GNSS stations in the USCB area is determined. The determined pattern of geodetic strain in the USCB area can explain the formation of high-energy seismic tremors that are not related to mining operations.

TECTONIC SETTING AND SEISMICITY

In strict geological terms, the Upper Silesian Coal Basin (USCB) is not a tectonic unit but this term is commonly used in the geological literature and hence also here. The boundary of the USCB is in fact an intersectional line that delimits the range of the Carboniferous deposits on the sub-Permo-Mesozoic and sub-Cenozoic surfaces in the area of the Upper Silesian Block (Fig. 1). Therefore, the USCB should be considered rather as a deposit and as an economic unit (Buła et al. 2008, Żelaźniewicz et al. 2011), as well as a complex group of geological units that comprise a foreland basin system connected with the Carboniferous Variscan orogeny (Kusiak et al. 2006). The tectonic position of the USCB area placed between the major tectonic units in this part of Europe and its geological significance in the geodynamic evolution of this region has been the subject of numerous papers (e.g. Doktorowicz-Hrebnicki 1963, Znosko 1965, Jura 1995, 2001, Botor et al. 2017).

This triangular shaped basin is placed within two main structural units of the Alpine complex: the Carpathian Foredeep in the south and the Silesian-Cracow Monocline in the north (Lewandowski 2007). The Upper Silesian Coal Basin is located in the Upper Silesian Block, and is a part of a larger tectonic unit – the Brunovistulia Terrane, an external part of the Bohemian Massif. In turn, the Bohemian Massif represents the easternmost Variscan unit of the European Platform evolved between the colliding Laurasia and Gondwana from the Devonian to Carboniferous. Many authors provided geophysical and GNSS data indicating a modern activity of this tectonic unit (Schenkova et al. 2009, Pospíšil et al. 2019, Roštínský et al. 2020, 2024).

In general, three structural zones are distinguished in productive Carboniferous structures (Idziak et al. 1999):

1) the folded tectonic zone, located in the western part of the basin and shaped as a narrow belt;
2) the block tectonic zone, situated to the east of the folded zone, where Carboniferous formations lie flat, but fault tectonics is particularly developed;
3) the fold-block tectonic zone, adjoining the block tectonics zone to the north and north-east directions.

The tectonic pattern in the USCB has mostly resulted from horizontal compression or from the presence of predominantly horizontal component of stress in the Variscan.

Fig. 1. *Geological and tectonic settings: A) main basement units surrounding the Upper Silesian Coal Basin (after Kusiak et al. 2006, Kroner et al. 2008); B) tectonic sketch of the USCB (after Buła & Kotas 1994, Mendecki et al. 2020)*

It was seen that the strike-slip movements occurred during the process of compressing (as movements in the Upper Silesian Trough) and related to the formation of longitudinal inversion structures (Doktorowicz-Hrebnicki 1963, Znosko 1965, Goszcz 1999, Dubiński et al. 2019). Numerous folds and depressions, thrusts and faults were superimposed on this structural arrangement. The following sub-units can be distinguished within the Upper Silesian Block: Upper Silesian Trough (UST), Upper Silesian Fold Zone, Moravo-Silesian Fold-and-Thrust Belt, Bielsko-Biała Dome, Rzeszotary Horst and Liplas Graben (Żelaźniewicz et al. 2011). The USCB developed on the rocks of the pre-Cambrian consolidation, and it is mostly located in the Upper Silesian Trough. The northern part of the USCB is already within the Upper Silesian Fold Zone and the western part belongs to the Moravo-Silesian Fold-and-Thrust Belt (Buła & Kotas 1994, Buła et al. 2008).

While all research on the subject has indicated a significant role of Variscan tectonics in the structural development of the basin (see for example Ptáček et al. 2012), the influence of Alpine-Neogene tectonic movements is controversial.

One group of authors has considered these factors to be insignificant (Jureczka & Kotas 1995), while another author has set out proof to show the importance of the intensive faulting and strong tectonic disturbances in the Miocene sediments in the southern part of the area (Aleksandrowicz 1964), while some others have found analogous phenomena in Quaternary sediments and landforms (Dyjor et al. 1978, Herbich 1981, Kotlicka 1981, Lewandowski 1995). Other investigations, based on the *in situ* measurements, have shown that the recent stress state in the southern part of the USCB (in Karviná Sub-basin) is influenced by the stress fields of the Outer Western Carpathian nappes front (Ptáček et al. 2012).

Recent tectonic movements were also detected by some authors through investigations of seismic events (Teper et al. 1992, Teper 1998, Idziak et al. 1999). The phenomena have been caused by the interaction of the tectonic stresses existing in the area under study with the mining-induced stress (Zuberek et al. 1996). According to Teper (1998) the present-day seismicity in the area can be governed by tectonic stress in the zones of large active dislocations (as found in the Kłodnica Fault, the central part of the basin). The source of this stress is derived either from the Carpathians orogenic pressure or from the active fractures in the Carboniferous bedrock.

Analysis of the seismic activity of the USCB area shows that it is a variable regardless of mining activity and, paradoxically, an increase in activity is noticeable despite the decline in coal extraction (Patyńska & Stec 2017, Szczerbowski 2019). The specificity of the area is the occurrence of numerous tremors with energy $E \geq 10^5$ J, which are difficult to explain by mining operations. It is commonly assumed that tectonic stresses, current or residual, may contribute to the generation of such phenomena (Teisseyre 1983, Gibowicz 1990, Zuberek et al. 1996, Patyńska & Stec 2017). The high energy tremors have not occurred uniformly throughout the whole area of the Upper Silesian Coal Basin but were concentrated in several areas belonging to different structural unit (Patyńska & Stec 2017): The Main Saddle (the northern part of the USCB), the Main Trough (the central part of the USCB), the Jejkowice and Chwałowice Trough (the western part of the area), the Bytom Trough (the northern part of the area) and the Kazimierz Trough (the northern part of the area).

Detailed analyses of epicentres provided surprising results which may be evidence that the seismicity of the basin is of a regional nature (Idziak et al. 1999):

- It has been shown that the epicentres of successive shocks are not randomly distributed, but are arranged in accordance with certain directional trends. Analysing the time sequences of strong shocks in the area of the Main Saddle and the Bytom Basin, it was found that the occurrence of foci alternates, i.e. the occurrence of a strong shock, e.g. in the Main Saddle, will with high probability cause a strong shock in the Bytom Trough.
- The distribution of the shock epicentres is self-similar in the statistical sense and creates a random fractal set with a diverse fractal dimension in the individual structural sub-units of the USCB.

Since it is assumed that these high-energy tremors are caused by the interaction of mining-induced stresses and tectonic stresses, the question arises as to how these stresses might affect the ground surface. The use of geodetic data to determine the regime of horizontal deformation in the USCB is a matter that has not been analysed so far.

THE MATHEMATICAL EXPRESSION OF THE DEFORMATION FIELD

Taking into consideration that the data are a GPS/GNSS measured velocity of the station, the present analysis is dealing here with the two-dimensional velocity gradient tensor. Collection of the velocities allows us to calculate with the two-dimensional velocity. So, a local displacement field around a given point $P(x, y)$:

$$\delta(x,y)=\begin{bmatrix} u(x,y) \\ v(x,y) \end{bmatrix} \tag{1}$$

The consider tensor which is defined as (Michel & Person 2003, Allmendinger et al. 2012, Sigbjörnsson et al. 2018):

$$u_i = u_i^0 + \frac{\partial u_i}{\partial u_j} x_j = u_i^0 + e_{ij} x_j \tag{2}$$

where:

- u_i – the GPS/GNSS velocity determined for the station,
- $u^0{}_i$ – a constant of integration that corresponds to the displacement at the coordinate system origin,
- x_j – the position of the station,
- e_{ij} – the displacement rate (velocity) gradient tensor.

There are six unknowns in two dimensions: two components of the translation vector (t_1, t_2), and four components of the displacement gradient tensor or deformation gradient tensor (e_{11}, e_{12}, e_{21}, e_{22}), so the solution of the constructed system of equations requires data from at least three non-colinear stations ($n \geq 3$). Solving these equations starts with the effects and then calculates the causes and a standard least squares solution to the over-constrained problem is usually used. One gets rid of the reference to the relative change in the displacement field that was used to calculate it. The interpretation of such a tensor can be ambiguous, but its decomposition can help to reveal certain characteristics. The approach presented here is valid for small displacements and velocities – the general formulas for strain rate reduce to the above-given equation for e_{ij}. So, for infinitesimal strains, tensor ε can be decomposed into symmetrical and antisymmetrical parts, into a strain rate and a rotation rate respectively (Cronin et al. 2012):

$$e_{ij} + \varepsilon_{ij} + \omega_{ij} = \left(\frac{\varepsilon_{ij} + \varepsilon_{ji}}{2}\right) + \left(\frac{\varepsilon_{ij} - \varepsilon_{ji}}{2}\right) =$$

$$= \begin{bmatrix} e_{ux} & \frac{e_{uy} + e_{vx}}{2} \\ \frac{e_{uy} + e_{vx}}{2} & e_{vy} \end{bmatrix} + \begin{bmatrix} e_{ux} & \frac{e_{uy} - e_{vx}}{2} \\ \frac{-\left(e_{uy} - e_{vx}\right)}{2} & e_{vy} \end{bmatrix} = \quad (3)$$

$$= \begin{bmatrix} \varepsilon_{ux} & \varepsilon_{uy} \\ \varepsilon_{vx} & \varepsilon_{vy} \end{bmatrix} + \begin{bmatrix} 0 & -\omega_z \\ \omega_z & 0 \end{bmatrix}$$

where:

- ε_{ij} – the infinitesimal strain rate tensor,
- ω_{ij} – the rotation rate (vorticity) tensor.

Hence, considering the previously mentioned formulas and using Einstein's summation convention, the formula, the velocity field can be expressed as follows:

$$u_i = u_i^0 + \frac{\partial u_i}{\partial u_j} x_j = u_i^0 + e_{ij} x_j \quad (4)$$

The stated terms on the right-hand side of the formula refer respectively to: translation, rotation (the antisymmetric deformation tensor), the rate of strain (symmetric tensor of deformation, also called Cauchy's tensor). The first two relate to rigid-body motion and the last term describes the rate of strain due to the relative velocity of the points.

The antisymmetric tensor can be understood as a rotation ω_{xy}. This rotation is composed by a rigid rotation Ω which affects the whole area and a differential rotation or twist $\delta\omega_{xy}$ (Michel & Person 2003). Differential rotation values grow with the deformation amplitude:

$$\delta\omega = \omega_z - \Omega = -\frac{e_{uy-}e_{vy}}{2} - \Omega \quad (5)$$

The complete matrix equation expressing the deformation at an individual site given its initial location $\{x_0, y_0\}$, translation velocity vector (t_x, t_y), the corresponding X (v_x) and Y velocity component (v_y), the magnitude of the angular velocity vector (Ω) and the elements of the strain rate tensor to be computed (ε_{xx}, ε_{xy}, ε_{yx}, ε_{yy}) is as below (Cronin et al. 2012):

$$\begin{bmatrix} v_x \\ v_x \end{bmatrix} = \begin{bmatrix} \varepsilon_{xx} & \varepsilon_{xy} - \Omega \\ \varepsilon_{xy} + \Omega & \varepsilon_{yy} \end{bmatrix} \begin{bmatrix} x_0 \\ y_0 \end{bmatrix} + \begin{bmatrix} t_x \\ t_y \end{bmatrix} \quad (6)$$

So, after unpacking there are two equations with six unknowns: t_x, t_y, Ω, ε_{xx}, ε_{xy} and ε_{yy} for each station:

$$\begin{aligned} v_x &= \left(x_0\varepsilon_{xx}\right) + \left(y_0\varepsilon_{xy}\right) - \left(y_0\Omega\right) + \left(t_x\right) \\ v_y &= \left(x_0\varepsilon_{xy}\right) + \left(x_0\Omega\right) + \left(y_0\varepsilon_{yy}\right) - \left(t_y\right) \end{aligned} \quad (7)$$

Entering the horizontal velocities (v_x and v_y) for three stations there will be six equations (two for each site) and the solving of these six equations is all that is necessary to solve this system of equations with six unknowns and such constraints to yielding an exact solution.

The six equations can then be expressed in a single matrix equation:

$$\mathbf{d} = \mathbf{G}\,\mathbf{m} \quad (8)$$

where:

- **d** – the matrix of the known velocity components for the three stations,
- **m** – the matrix of the six unknowns,
- **G** – the matrix of coefficients that relates **d** to **m** using the aforementioned equations.

To derive the model parameters in matrix m, there is an inverse problem to be solved and the known quantities should be collected on one side and the unknowns on the other side of the equation:

$$\mathbf{m} = \mathbf{G}^{-1}\mathbf{d} \tag{9}$$

Calculation of the matrix **m** provides six components which include the coordinates of the translational velocity vector (in meters per year), the rotational velocity (in radians per year), and the three dimensionless elements of the strain matrix.

The symmetric tensor is a symmetric matrix and is usually represented by an ellipse with the following parameters. There are the following primitive quantities defined by the deformation tensor which represent and characterize the deformation (Michel & Person 2003, Cronin et al. 2012):

- the eigenvectors determining the direction of the principal axes,
- the eigenvalues determining the length of the semi-axes:

$$eigenvalues = \frac{\left(\varepsilon_{xx}+\varepsilon_{yy}\right) \pm \sqrt{4\varepsilon_{xy}\varepsilon_{yx}+\left(\varepsilon_{xx}+\varepsilon_{yy}\right)^2}}{2} \tag{10}$$

The eigenvalues of ε_{xy} are the principal extensions in the principal directions. The larger eigenvalue e_1 corresponds to the greater principal extension along the greater horizontal strain axis $S_{1H} = e_1 + 1$. The smaller eigenvalue e_2 is the lesser principal extension along the lesser horizontal strain axis $S_{2H} = e_2 + 1$.

An eigenvector corresponding to e_1 is:

$$\left\{1, \frac{e_1-\varepsilon_{11}}{\varepsilon_{12}}\right\} \tag{11}$$

An eigenvector corresponding to e_2 is:

$$\left\{1, \frac{e_2-\varepsilon_{11}}{\varepsilon_{12}}\right\} \tag{12}$$

The unit eigenvectors can then be determined by dividing each of the components of these vectors by their length or norm. For example, the unit eigenvector associated with eigenvalue e_1 is as follows (Cronin et al. 2012):

$$\widehat{S_1} = \left\{ \frac{1}{\sqrt{1+\left(\frac{\lambda_1-\varepsilon_{11}}{\varepsilon_{12}}\right)^2}}, \frac{\frac{\left(\lambda_1-\varepsilon_{11}\right)}{\varepsilon_{12}}}{\sqrt{1+\left(\frac{\lambda_1-\varepsilon_{11}}{\varepsilon_{12}}\right)^2}} \right\} \tag{13}$$

The azimuth of the S_{1H} axis is related to the angle between the unit north vector and the unit vector that coincides with this axis is:

$$\Theta_{[\mathrm{rad}]} = \left(\cos^{-1}\left(\hat{n}\cdot\widehat{S_1}\right)\right) \tag{14}$$

If the value of the x coordinate of the S_1 eigenvector is a negative number, then the absolute values of Θ is subtracted from 360° to yield the azimuth. If it is not a negative number, the azimuth equals to Θ.

Based on the quantities more meaningful parameters can be evaluated and their values can be estimated using geodetic data of three different GPS/GNSS stations: maximum horizontal extension, minimum horizontal extension, total velocity, maximum shear strain, area strain and rotation (Lazos et al. 2018, 2020). So, the parameters commonly used in the interpreting of geodetic data within deformation study are as follows:

- The maximum (e_{1H}) and minimum (e_{2H}) horizontal extensions, they are measured along the longest and shortest axes of the strain ellipse, respectively. An extension is dimensionless (usually expressed in nanostrains, nε) and for the maximum horizontal extension it is defined as $(l_t - l_0)/l_0$, where l_t is the final length and l_0 is the original length along the major axe of the strain ellipse. The minimum horizontal is defined correspondingly: $(l'_t - l'_0)/l'_0$, where l'_t is the final length and l'_0 is the original length along the minor axe of the strain ellipse.
- The maximum shear strain (γ_{max}) which is measured at 45° from the maximum horizontal strain axis is equal to the difference between the extension (e_{1H}) along the major axis (S_{1H}) and the extension (e_{2H}) along the minor axis (S_{2H}) of the ellipse: $e_{1H} - e_{2H}$. It is expressed in nanostrains, and the magnitude of the infinitesimal shear strain as well can be given by the following:

$$\gamma_{\max} = 2\sqrt{\frac{\varepsilon_{xx} - \varepsilon_{yy}}{2} + (\varepsilon_{xy})^2} \quad (15)$$

- The area strain depicts the change in area size as a result of distortion (if any), so it is a parameter characterizing the type of tectonic regime of an area. The area strain is equal to the sum of the aforementioned extensions: $\Delta = e_{1H} + e_{2H}$ and is expressed in nanostrains. In particular, the types of area strain are dilatation and compaction.
- Rotation is a parameter which mathematically is defined as being the angle between the major (or minor) axis of the undeformed figure which is assumed to be deformed (circle, triangle) and the major (or minor) axis of that figure after its deformation. It is expressed in nanoradians per year.

The quantitative property of the deformed area can be expressed in the above-mentioned parameters which should be considered as a product of the measurement process. So analysis of the results requires the determination of one more parameter – that of measurement uncertainty which is "associated with the result of a measurement that characterizes the dispersion of the values that could reasonably be attributed to the measurand" (JCGM 2008). Therefore, we can see that the uncertainty of strain estimate is a function of the individual uncertainties in the velocity estimates (usually attributed to the GPS/GNSS data) and the propagation of these uncertainties affecting the model space (Cronin et al. 2012).

Data uncertainty can be expressed as a covariance matrix cov(**d**) with diagonal values equal to individual variances (σ^2), assuming that the error in estimating the velocity of each station is independent of the other stations (Cronin et al. 2012). So, for the equation $\mathbf{m} = \mathbf{G}^{-1}\mathbf{d}$ the covariance of the model cov(**m**) can be expressed as (Cronin et al. 2012):

$$\text{cov}(\mathbf{m}) = (\mathbf{G}^T \text{cov}(\mathbf{d})^{-1} \mathbf{G})^{-1} \quad (16)$$

where the inverse of the data covariance matrix $\text{cov}(\mathbf{d})^{-1}$ is simply a diagonal matrix whose only non-zero terms are along the diagonal of the matrix with values equal to $1/\sigma^2$ for each estimate of the station velocity (uncertainties in the site velocities). The product of the formula is a covariance matrix cov(**m**) with the diagonal elements which are the variances (σ^2) for each of the model parameters that were to be estimated. Taking the square root of each of the variances (the diagonal values) in successive rows of the matrix, the estimated uncertainty for the parameters as follows: for the east-west and north-south components of translation vector (respectively), for the angular velocity vector, ε_{xx}, ε_{xy} and ε_{yy}.

ESSENTIALS OF THE TRIANGULATION METHOD

Strain-rate studies using GPS/GNSS data are characterized by some specific features. The first feature of strain rate based on GPS/GNSS data is the source of the data on which the strain is based. The basis of the measurement is the velocity of GPS/GNSS stations, and more precisely the diversity of their distribution. So, the velocities measured at the three GPS/GNSS sites which are located in a tectonic active area provide a deformation of the triangle which they form and the deformation is the result of three components: translation, rotation, and distortion of the crust – deformation rate = translation rate + rotation rate + distortion rate.

The second specific aspect is the expression of geodetic data as a physical property of a geosystem that can be quantified by measurement. However, strain being a dimensionless quantity, the GPS/GNSS results (initially velocities) after processing actually express strain velocity as a "per year" number. The units used in infinitesimal strain-rate studies using GPS/GNSS data are usually nanostrains per year, even though the element "strain" itself has no dimension.

The third feature is related to the sometimes overlooked aspect of the certainty that movements caused by tectonic process are actually reflected by the geodetic data. GPS/GNSS measurements do not always reflect pure tectonic activity but they may be affected by a variety of non-tectonic processes including ground movements resulting from changes in the hydrogeological regime, displacements caused by anthropogenic sources

or by artificial effects resulting from this satellite technique (e.g., Segall & Davis 1997, Szczerbowski & Jura 2015, Krawczyk & Grzybek 2018, Witkowski et al. 2021, Overacker et al. 2022).

Ground displacements induced by the seasonal variations of subsurface water reservoirs usually follow a seasonal pattern but these may vary in amplitude from year to year and do not usually follow a simple sinusoidal characteristic with respect to frequency. This is often called a quasi-seasonal pattern and is often removed from continuous GPS/GNSS observations in deformation studies (Bawden et al. 2001, Blewitt et al. 2001, Heki 2001, Schmidt & Bürgmann 2003, Argus et al. 2005, Bogusz et al. 2013).

Hence the environmental conditions should be considered as an individual characteristic of a given area in geodetic studies devoted to strain field. In this paper the problem is discussed with the use of individual sets of data obtained from particular stations.

The above-mentioned symbolic solutions to strain problem can be depicted geometrically and the triangulation method is an approach which perfectly combines both of the aspects of tectonic strain. We can see why it is a common method applied in geodetic studies on tectonic strain that is a common method applied in geodetic studies on tectonic strain. As the name suggests, triangulation consists of creating a system of triangles covering the area under consideration and in this case the vertices of the triangles represent the permanent GPS/GNSS stations. Sets of three stations in the study area are combined, forming a triangle, while the velocities of the three stations are taken into account in order to calculate the deformation parameters. Reliability of the results depends on the aforementioned uncertainty of strain estimate and also on the correct alignment and positioning of the network of GPS/GNSS stations.

The procedure starts from the determination position of the centroid (C) of the triangle. The vector from the centroid of the undeformed triangle (C) to the centroid of the deformed triangle (C′) is the same as the translation vector. The translation vector can be outlined by the East and the North components or the azimuth of the translation which is the average direction in which the GPS/GNSS sites are moving. Also taken into consideration is the velocity of the translation vector which is the length or magnitude of the vector, expressed in meters per year.

The translation vector has the same magnitude and direction at all the three stations and the centroid of the triangle which they formed is the intersection of three triangle medians. This point is considered as the starting point (x_0, y_0) of a new coordinate system and the triangle of the stations simply moves in space relative to the reference frame. The triangle deforms as it moves. Subsequently, an inner circle with the centre in the centroid is contained in the original and undeformed triangle. It is transformed into an ellipse when positions of the triangle vertices (stations) change due to the relocation of each vertex from the starting to the finishing point of each total horizontal velocity vector (Fig. 2).

The strain ellipse and its axes (a major and a minor axis), perpendicular to each other, describe the magnitude and orientation of the maximum and minimum principal strain.

Subtracting the translation vector from the velocities of the triangle vertices brings the two triangle centroids together. The site velocities minus the translation vector makes the site vectors associated with the change into the shape of a triangle. The reversal of the deformed triangle into its original position leads to the transformation of the ellipse into a circle, while the ellipse axes remain perpendicular to each other, however slightly they may have changed. So, as mentioned before, the rotational component of deformation is indicated by the angular change in orientation per year and the direction of the rotation is calculated from the original orientation of the given axis and its orientation after deformation (Fig. 2). A positive rotation is a counter-clockwise rotation (Cronin et al. 2012, Lazos et al. 2018, 2020).

The rotational velocity vector (an axial vector, angular velocity vector) is a vertical vector extending from the centre of the triangle. It can be given in degrees per year or in billionths of a radian per year (nrad/yr). In the case of a rigid body its rotating is possible but there is no presence of any distorting component. Distortion is the next quantity that appeared in the previously presented formula and it includes a change in shape (strain) as well as some change in volume/area (dilation).

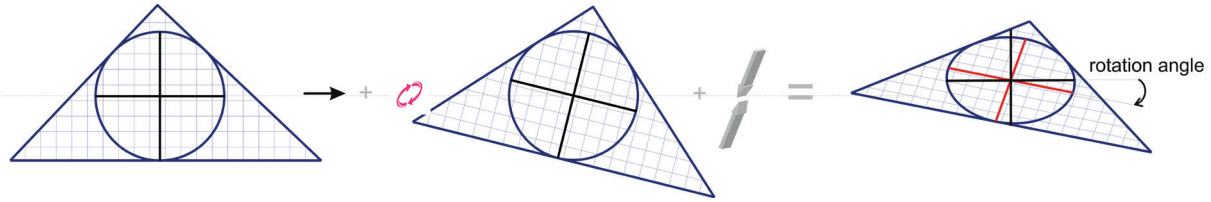

Fig. 2. *Defining deformation: a forward deformation deforms a unit circle to a strain ellipse. Successive figures from the top to the bottom: initial configuration of GNSS triangle with circle around the centroid of the triangle, rotation of the triangle, deformed triangle with circle and ellipse as a product of the changed circle with the major axis with clockwise rotation and which trends 105° (minor axis is red perpendicular). For irrotational deformation, the axes which transform to become the principal strain axes (dashed) are not rotated*

The implementation of this process, using different mathematical equations including the original and final lengths of the ellipse axes, leads to the estimation of the parameters discussed in the previous chapter. In the present paper, the triangulation method as algorithms applied in the computation process are based on the GPS/GNSS triangular calculator software, developed by EarthScope and presented among others in many publications (see: Cronin et al. 2012). All strain parameters which can be determined on the mentioned formulas with the use of the software are examined here to detect tectonic trace in geodetic signals recorded in the stations to identify tectonic regime in the area of the USCB.

ESTIMATION OF INFINITESIMAL STRAIN USING GPS/GNSS VELOCITY DATA GATHERED FROM SITES IN A TRIANGULAR ARRAY

To achieve a full understanding of the extent of present-day crustal strain in a given area not only requires the relevant geological/geophysical data, but also information gathered from many locally available GPS/GNSS sites. In the case under discussion, the geological structure of the area is well recognized, but the geophysical research of the tectonic stress has been insufficient and has been limited only to seismic research.

Unlike campaign (occasional) measurements, continuous measurements performed at permanent GNSS stations provide unique data sets for rigorously assessing ground deformation, especially valuable in regions of low displacement rates. The permanent stations which are in operation in the area of Poland are developed and managed by various companies or institutions belonging either to public or commercial networks (ASG-EUPOS, TPI NETpro, VRSNet HxGN SmartNet and local networks covering the southern part of Poland: NadowskiNET, RtkNet). Some of these networks are operating in the area under study, however most stations belong to the ASG-EUPOS network, which was established in 2008 according to the guidelines set down by the Polish Head Office of Geodesy and Cartography (Bosy et al. 2007). There are three stations operating in the area of the Czech Republic (one of them – the CFRM station belongs to the ASG-EUPOS network) and one in the Slovak Republic.

In the case under discussion here most of the operating GNSS stations are placed in urbanized locations of the region, where mining has not been conducted for many years. But while the influence of mining on the displacement field revealed by the geodetic data can be ruled out due to the ending of coal mining operations there, the influence of other man-made sources cannot be excluded.

The geodetic data were obtained from the Nevada Geodetic Laboratory (NGL) which takes raw GPS data from more than 17,000 stations around the globe and makes data products that are multi-purpose (Blewitt et al. 2018). The processed data available from the NGL site give the daily averages of displacements relative to the initial position of the station and these have been resolved in a particular reference frame and are relative to a particular datum. The data obtained

from the stations operating in the study area within the various Polish and Czech networks were calculated by the Geodesy Lab at the University of Nevada (NGL) to provide coordinates computed from a time series which comprised of many of these daily displacements and hence provided the mean velocities in the north and the east directions in time intervals for the analysed stations (more useful pieces of information are available at http://geodesy.unr.edu). The GPS/GNSS site locations and velocity data relative to a fixed Eurasian plate presented here, which were obtained from NGL (Blewitt et al. 2018), encompass the velocity rates which were calculated with respect to the stable Eurasia plate. Each analysed station is characterized by an East and a North velocity component and their errors, respectively (Table 1).

The input data give positions of GNNS sites and their velocities, expressed in units of length per time, i.e. per one year. The GNSS data acquisition in the USCB and adjacent areas and the analysis process, according to infinitesimal strain theory, deals with very small displacements (indeed, infinitesimally smaller than any relevant dimension of the examined area). However, as is shown, the velocities in the study area are much lower than those usually found in regions of active faulting, for example in the area of the North Anatolian fault, where the Arabian plate moves northward about 20 mm/yr with respect to Eurasia (Allmendinger et al. 2007). The values of the velocity vectors vary from 0.5 to 2.7 mm/yr. Therefore, the values should be considered as being significant and useful for further analysis despite the small values which they depict. What is more, the values of the uncertainties as well are much diversified. The stations of the ASG-EUPOS network have provided data of a very good quality since 2004: they are the result of a long period of time of observations (almost two decades) coupled with a very low set of values of the uncertainties ranging up to ±0.2 mm (with the exception of TAR4 which started to operate several years later than the other stations of the network). These are the stations as follows: CFRM, KATO, KRAW, TAR4, WODZ, ZYWI. Some of the stations' names are different in the NGL service than the name used in the ASG-EUPOS nomenclature.

Table 1
Locations and velocities for GNSS/GPS stations used in this study

Station ID	Latitude [°]	Longitude [°]	E velocity [mm/yr]	E velocity uncertainty [mm/yr]	N velocity [mm/yr]	N velocity uncertainty [mm/yr]
ANDY	49.858	19.373	0.64	0.26	0.11	0.30
BEDZ	50.345	19.159	0.59	0.58	–1.54	0.72
CAD2	49.435	18.785	0.18	0.46	0.90	0.40
CFRM	49.685	18.353	–0.07	0.12	0.96	0.13
JASZ	49.916	18.495	0.48	0.26	–0.02	0.27
KATO	50.253	19.036	0.73	0.13	–2.60	0.15
KEDZ	50.375	18.331	0.24	0.25	0.72	0.30
KRAW	50.066	19.920	0.18	0.12	0.61	0.14
LYSH	49.546	18.448	0.11	0.17	0.86	0.18
OLKU	50.331	19.550	0.77	0.26	1.29	0.28
RACZ	50.078	18.215	0.92	0.32	0.54	0.37
TAR4	50.452	18.858	0.16	0.43	1.15	0.47
TYCH	50.119	19.009	0.04	0.37	2.57	0.57
VSBO	49.834	18.164	0.53	0.13	0.61	0.14
WODZ	50.000	18.458	0.00	0.35	2.04	0.30
ZYWI	49.687	19.206	0.06	0.14	1.01	0.15

The VSBO, a public station in the Czech Republic, has also provided high quality data (details are available on the website: http://czepos.cuzk.cz). The other stations are usually characterized by higher values of uncertainties and by a shorter time interval of observations. The NGL provides data from the other station networks placed in the area, but their published data are characterized by values of uncertainty which are several times higher than estimations of the velocity components and the published interval time of their operation is over a time period of several months, too short a time to be regarded as reliable.

Nearly half of the stations located in the USCB and adjacent zones demonstrate significant values of velocity rates of over 1 mm/yr: ZYWI, RACZ, TAR4, OLKU, BEDZ, WODZ, TYCH, KATO. The first four stations are located nearby, but still outside the boundaries of the area of the USCB, and the velocity rates of the last three stations exceed even 2 mm/yr. Detailed discussion on the characteristics of the spatial distribution of velocity vectors is presented further.

The calculation of the deformation parameters is based on the triangulation methodology described previously. Triples of the neighbouring stations formed triangles. As can be seen, their distribution is not perfect and differences in the density of station locations caused significant irregularity in the geometry and area size of the triangles. Despite this, however, their positions match the geological situation quite well. Table 2 shows the results obtained from the calculations for each of the triangles, including values of uncertainty evaluated for elements of the strain rate tensor, and for components of the translation vector.

Although the triangles were formed according to the principle of nearest position, triangles being formed by neighbouring stations, some triangles were established in which geometry set aside this standard to reveal additional insight into a very diverse picture of strain distribution within the USCB area. The results should be considered as being assigned to the centroid of the triangle. Thus, deformation parameters were determined for each centroid of the triangle, the most considerable of them being as follows:

- Maximum horizontal extension. The values range from –10 to 330 nε but most of the triangles manifest values in the range from 5 to 70 nε which is approximately the mean value of the data set. One triangle (T4) shows a negative value (–10 nε).
- Azimuth of maximum horizontal extension. The values of the data almost evenly fill the full range of the circular angle and in terms of frequency no preferred direction can be seen.
- Minimum horizontal extension. The values for the majority of the triangles amounted to the range from –40 to –10 nε. The mean value of the data set is –80 nε, so the values of the modulus of the means of maximum and minimum horizontal extensions are nearly identical.
- Velocity of the centroids. The values correspond to those obtained for the stations forming a particular triangle and the rates are ranging between 0.4 and 1.8 mm/yr.
- Maximum shear strain. The values range from –10 to 790 nε but most of the triangles manifest values in the range of 10 to 80 nε. That resembles the range obtained for maximum horizontal extension. For three triangles (T6, T11, T12) obtained values are remarkable as they exceed 400 nε.
- Rotation. The mean and the median are both close to zero and that reflects a dominant tendency in the data set. Three triangles provide outstanding values: T6 (ca. 32 mas/yr), T11 (ca. –80 mas/yr), T12 (ca. 57 mas/yr). So only T11 demonstrates a clockwise rotation, while the other two demonstrate an anti-clockwise rotation. Although the determined values are characterized by high uncertainty values, they reflect anomalies in the velocity field. Nothing prevents these results from being analyzed as being qualitative.
- Area strain. The values vary in the range of –500 to 451 nε. Again, T11 and T12 provide outstanding values (respectively –525 and –128 nε). The mean and the median of the modulus values are close to zero. However, despite the fact that the absolute values of negative area strain rates are much higher than positive ones the latter are dominant, and the highest positive value is demonstrated by T21. Overall, it reflects an extensional nature of the USCB area if it is viewed as a whole.

Table 2
Compilation of evaluated strain rates

Triangle	Translation vector		Velocity [mm/yr]	ε_{xx} ± uncert. [nε]	ε_{xy} ± uncert. [nε]	ε_{yy} ± uncert. [nε]	Rotation ± uncert. [mas/yr]	Direction of rotation	Max. horizontal extension [nε]	Azimuth of max. horizontal extension [degrees]	Min. horizontal extension [nε]	Max. shear strain [nε]	Area strain [nε]
	E component ± uncert. [mm/yr]	N component ± uncert. [m/yr]											
T1 (LYSH-CAD2-ZYWI)	0.12 ±0.2	0.92 ±0.2	0.9	0.31 ±7.7	−1.19 ±12.8	1.31 ±21.7	0.74 ±12.8	anti-clockwise	2.11	146.38	−0.482	2.59	1.62
T2 (LYSH-CAD2-JASZ)	0.26 ±0.2	0.58 ±0.2	0.6	7.37 ±20.3	−0.64 ±9.9	−20.36 ±7.3	−1.82 ±9.9	clockwise	7.39	91.33	−20.371	27.76	−12.98
T3 (LYSH-CFRM-JASZ)	0.17 ±0.1	0.60 ±0.1	0.6	39.44 ±23	−24.56 ±12.8	−15.22 ±8.1	−5.98 ±12.8	clockwise	48.85	110.97	−24.638	73.49	24.21
T4 (VSBO-CFRM-JASZ)	0.31 ±0.1	0.52 ±0.1	0.6	−11.21 ±10.8	5.74 ±7.3	−32.06 ±9.6	−4.31 ±7.3	clockwise	−9.73	75.58	−33.535	23.80	−43.26
T5 (VSBO-RACZ-JASZ)	0.64 ±0.1	0.38 ±0.2	0.7	−7.48 ±12.9	−5.55 ±9.6	2.06 ±15.4	−4.39 ±9.6	clockwise	4.61	155.34	−10.023	14.63	−5.42
T6 (WODZ-RACZ-JASZ)	0.47 ±0.2	0.85 ±0.2	1.0	−94.23 ±54.6	82.25 ±38.7	277.74 ±53.7	32.29 ±38.7	anti-clockwise	295.12	11.93	−111.604	406.72	183.52
T7 (WODZ-RACZ-KEDZ)	0.39 ±0.2	1.10 ±0.2	1.2	−56.27 ±27.5	36.97 ±15.1	−17.22 ±10.0	8.55 ±15.1	anti-clockwise	5.06	31.08	−78.555	83.61	−73.50
T8 (WODZ-TYCH-KEDZ)	0.09 ±0.2	1.78 ±0.2	1.8	−0.68 ±10.8	13.60 ±9.2	−27.51 ±10.8	1.65 ±9.2	anti-clockwise	5.01	67.30	−33.200	38.21	−28.19
T9 (TAR4-TYCH-KEDZ)	0.15 ±0.2	1.48 ±0.3	1.5	−2.61 ±10.9	10.22 ±10.5	−33.38 ±21.0	1.59 ±10.5	anti-clockwise	0.47	73.20	−36.467	36.94	−36.00
T10 (TAR4-KATO-KEDZ)	0.38 ±0.2	−0.24 ±0.2	0.4	2.55 ±9.2	−21.55 ±13	156.61 ±26.0	0.50 ±13.0	anti-clockwise	159.57	172.18	−0.405	159.97	159.16

Table 2 *cont.*

T11 (TAR4-KATO-TYCH)	0.31 ±0.2	0.37 ±0.3	0.5	103.71 ±50	–356.70 ±35.3	–231.9 ±30.8	–79.81 ±35.3	clockwise	330.11	122.40	–458.293	788.40	–128.19
T12 (BEDZ-KATO-TYCH)	0.45 ±0.2	–0.52 ±0.3	0.7	–81.14 ±89.6	334.31 ±59.9	–443.57 ±51.2	56.75 ±59.9	anti-clockwise	117.91	59.23	–642.617	760.53	–524.71
T13 (BEDZ-KATO-OLKU)	0.70 ±0.2	–0.95 ±0.3	1.2	4.86 ±17.6	42.25 ±38.1	13.19 ±90.5	12.50 ±38.1	anti-clockwise	51.48	42.18	–33.425	84.91	18.06
T14 (BEDZ-KRAW-OLKU)	0.51 ±0.2	0.12 ±0.3	0.5	8.39 ±24.8	68.98 ±20.2	118.99 ±31.4	8.70 ±20.2	anti-clockwise	152.11	25.64	–24.720	176.83	127.39
T15 (KATO-KRAW-OLKU)	0.56 ±0.1	–0.23 ±0.1	0.6	–2.71 ±5.4	51.18 ±7.3	96.48 ±14.4	7.01 ±7.3	anti-clockwise	118.15	22.95	–24.383	142.54	93.77
T16 (TYCH-KRAW-OLKU)	0.33 ±0.2	1.49 ±0.2	1.5	4.79 ±6.6	–3.42 ±7.6	–3.73 ±13.7	–5.60 ±7.6	clockwise	5.99	109.40	–4.931	10.93	1.06
T17 (OLKU-KRAW-ANDY)	0.53 ±0.1	0.67 ±0.1	0.9	–15.21 ±6.7	3.11 ±5.2	22.59 ±7.8	–0.68 ±5.2	clockwise	22.85	4.67	–15.465	38.31	7.38
T18 (TYCH-KRAW-ANDY)	0.29 ±0.2	1.10 ±0.2	1.1	–0.11 ±5.4	–21.72 ±7.6	63.18 ±17.3	–0.29 ±7.6	clockwise	69.92	162.77	–6.845	76.77	63.08
T19 (TYCH-ZYWI-ANDY)	0.25 ±0.2	1.23 ±0.2	1.3	33.65 ±17.7	–38.77 ±11.7	9.22 ±10.6	–9.77 ±11.7	clockwise	62.09	126.26	–19.210	81.30	42.88
T20 (BEDZ-KATO-TAR4)	0.49 ±0.2	–1.00 ±0.3	1.1	7.91 ±42.8	–31.74 ±29.3	144.15 ±31.4	–2.19 ±29.3	clockwise	151.18	167.51	0.875	150.30	152.05
T21 (BEDZ-TAR4-OLKU)	0.51 ±0.3	0.30 ±0.3	0.6	4.15 ±30.4	54.65 ±55.1	446.85 ±126.3	16.94 ±55.1	anti-clockwise	453.50	6.93	–2.495	455.99	451.00
T22 (WODZ-TYCH-ZYWI)	0.03 ±0.2	1.87 ±0.2	1.9	1.04 ±10.4	1.58 ±7.9	33.12 ±14.8	0.35 ±7.9	anti-clockwise	33.20	2.82	0.967	32.24	34.17
T23 (KRAW-ZYWI-ANDY)	0.29 ±0.1	0.58 ±0.1	0.6	–46.63 ±24.6	62.84 ±21.3	–90.40 ±36.3	0.18 ±21.3	anti-clockwise	–1.97	54.60	–135.055	133.08	–137.03

RESULTS, ANALYSIS AND DISCUSSION

Once we obtain the requisite information from each of the GNSS sites, we know the horizontal coordinates of the initial site location (x_0, y_0) as well as the east-west instantaneous velocity (v_E) and the north-south velocity (v_N) for each site within a time interval which is not equal for all of the analysed stations. As mentioned previously, the velocity vectors which were obtained for the stations in the USCB, expressed in an EU plate-fixed reference frame, are rather small in comparison to areas with active fault tectonics and the strong effects of the movements they produce. The velocity field determined on the basis of the data presented in Table 1 outlines a complex characteristic of the vectors' distribution shown in Figure 3. Distribution of both the vectors' magnitudes and orientations within the USCB area are much diversified: neighbouring stations show velocity vectors of inverted orientation. It closely resembles microplate models of continental deformation where the deformation analysis is based on elastic block modelling which assumes that deformation is not continuous but occurs primarily in networks of interconnected faults separating quasi-rigid blocks (e.g., Avouac & Tapponnier 1993, Thatcher 2007, Allmendinger et al. 2007, 2009). The distribution of the velocity rates is outlined on the map in the form of arrows, with an orientation which determines the angle of the azimuth of the moving stations Figure 3A.

The distortion in the velocity vector field is far more easily perceptible on the map of the gradients (Fig. 3B). As is shown there are two distinctive zones: the first between WODZ and JASZ (the western part of the USCB), and the second between KATO and BEDZ stations (the central part of the USCB). The first shows much higher values of the gradient field. The areas with increased gradient values coincide with the locations of high-energy seismic events, which are shown in Figure 3C. A disturbance in the distribution of the velocity vectors in those zones results in a strong variability of the vectors and of the other deformation parameters obtained in the USCB area. These variabilities will be discussed further. It can be seen that the expected smooth and similar velocities of GNSS do not appear as such in the USCB. The lack of information on the velocities in some parts of the area does not preclude the formulation of certain remarks that in the western and the central parts extreme changes in the orientation of the vectors are observed. Even when ignoring the strong disturbance of the characteristics caused by the stations located in the mentioned zones, a change in the distribution of the vectors is already visible at the border of the USCB. However, the changes along the boundary of the area are much smoother and exhibit a certain regularity. The vectors of the CFRM, ZYWI, and KRAW stations – which surround the USCB area from the west, south, and east, respectively – show slight directional changes. These changes progress successively from SE–NW, through N, to SW–NE, in accordance with the curvature of the Carpathian arc, an adjacent tectonic unit. S–N orientation of the vectors is the dominating one in the surroundings of the area of the USCB, although this slight difference is noticeable: stations which are located at the western boundary of the region demonstrate SW-NE orientation. It suggests that this disturbance was originally created by the occurrence of the Basin. The directions of the vectors turn back to the S–N trend behind the northern boundary of the USCB and this orientation corresponds to the N–S orientation of the tectonic stress in the area of Poland, a phenomenon which has been discussed in numerous papers (e.g., Jarosiński 1998, 2005, 2006, Zuchiewicz et al. 2007, Jarosinski et al. 2011, Araszkiewicz et al. 2016).

The distribution of the maximum horizontal extension is analogous to the distribution of the values of the velocity. The maximal values of this parameter occur in the regions of the greatest disturbances caused by the velocity characteristics of the WODZ, KATO and TYCH stations (Fig. 4). The high values obtained for T14 and T21, which are the triangles covering zones not related to mining operations, are noticeable. Both occur at the northern boundary of the area, where the stations located beyond it (e.g., OLKU) show a northern direction of movement.

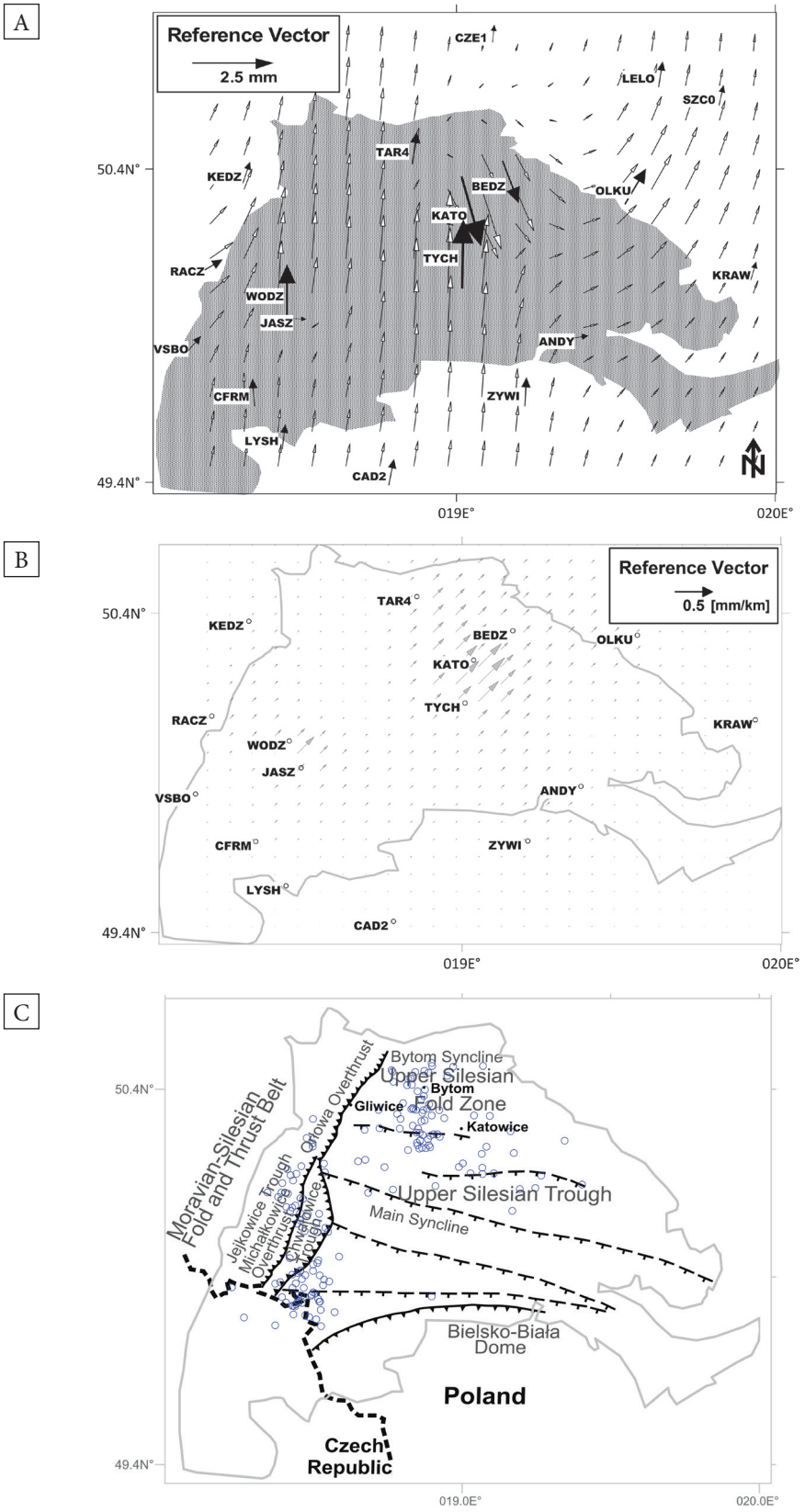

Fig. 3. *The GPS/GNSS horizontal velocity vectors determined for the stations operating in the USCB and in adjacent areas (arrows with black heads) and modelled the velocity field determined on the basis of the GNSS data (arrows with white heads) (A). The horizontal velocity gradient in the area evaluated on the basis of the horizontal velocity field (B). Location of high energy tremors occurred in the period from March 2000 to December 2024 (blue circles). Seismic data from USGS earthquake catalogue (https://earthquake.usgs.gov/earthquakes) (C)*

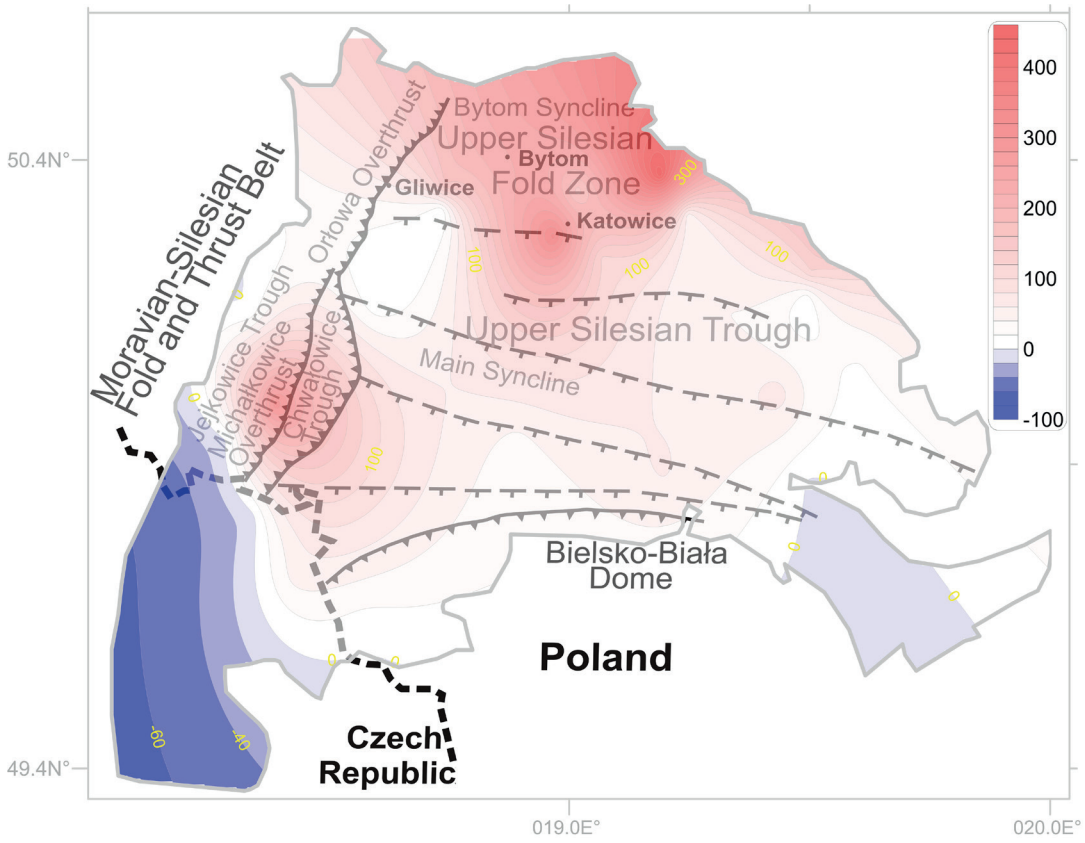

Fig. 4. *The Upper Silesian Coal Basin: the distribution of the maximum horizontal extension [nε]*

Those placed just in front of this boundary, however, demonstrate a diametrically opposite southward movement. Such a setting of the deformation causes extensional characteristics with large values of strain. This analogous tendency is also observed at the western boundary where the WODZ station located at the western boundary of the USCB demonstrates the northward displacements. The stations, however, located on its western side, on the Moravo-Silesian Fold-and-Thrust Belt, show movements from the west towards the centre of the USCB. A fairly even distribution of azimuths of maximum horizontal extension and the lack of the preferred directions in terms of frequency of the occurrence suggests the existence of forces acting in various directions. These directions seem to depend on the position of the particular triangle on the tectonic map of the USCB area. Taking into account the triangles which demonstrate the values of the maximum horizontal extension that exceed 100 nanostrains, it can be seen that these extensions represent the azimuths of orientation between NW and NE (frequently N).

So, as is shown in Figure 5 the azimuths of the large maximum horizontal extensions, placed in various zones of the area, represent, for the most part, a S–N direction. Less often SW–NE directions and only once a SE direction, which is demonstrated only by the T11 triangle.

The values of the minimum horizontal extension are negative and almost all of them are below 50 nε. Only three triangles demonstrated noteworthy values of the parameter: T6 (–112 nε), T11 (–458 nε) and T12 (642 nε). These are very large negative values, the modulus of which exceeds the corresponding values of the maximum horizontal extension several times. It suggests an extreme compressional regime in zones represented by the triangles, especially T11 and T12 (Fig. 6).

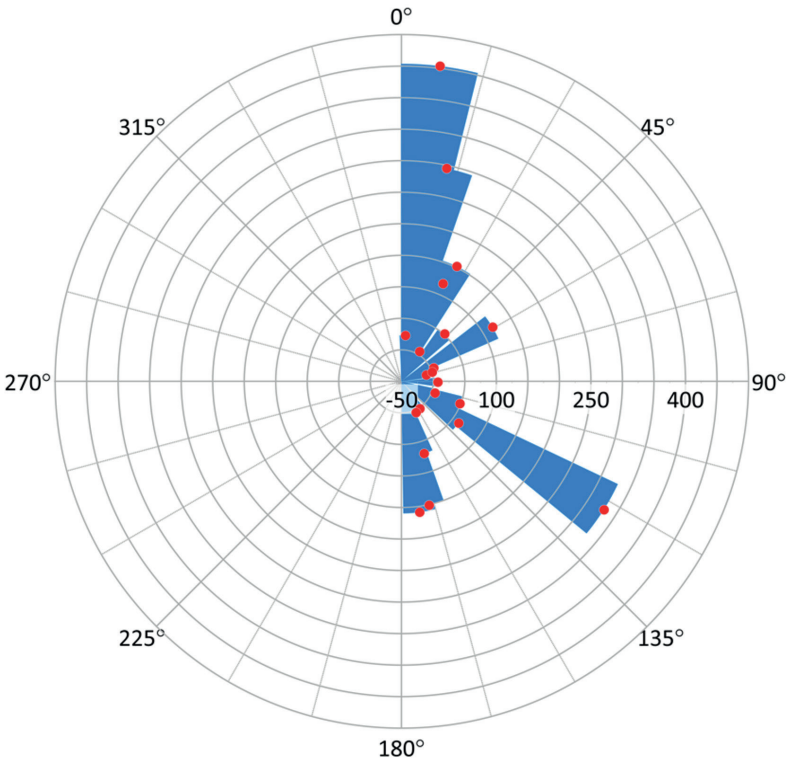

Fig. 5. *Diagram of azimuths of maximum horizontal extension [nε]*

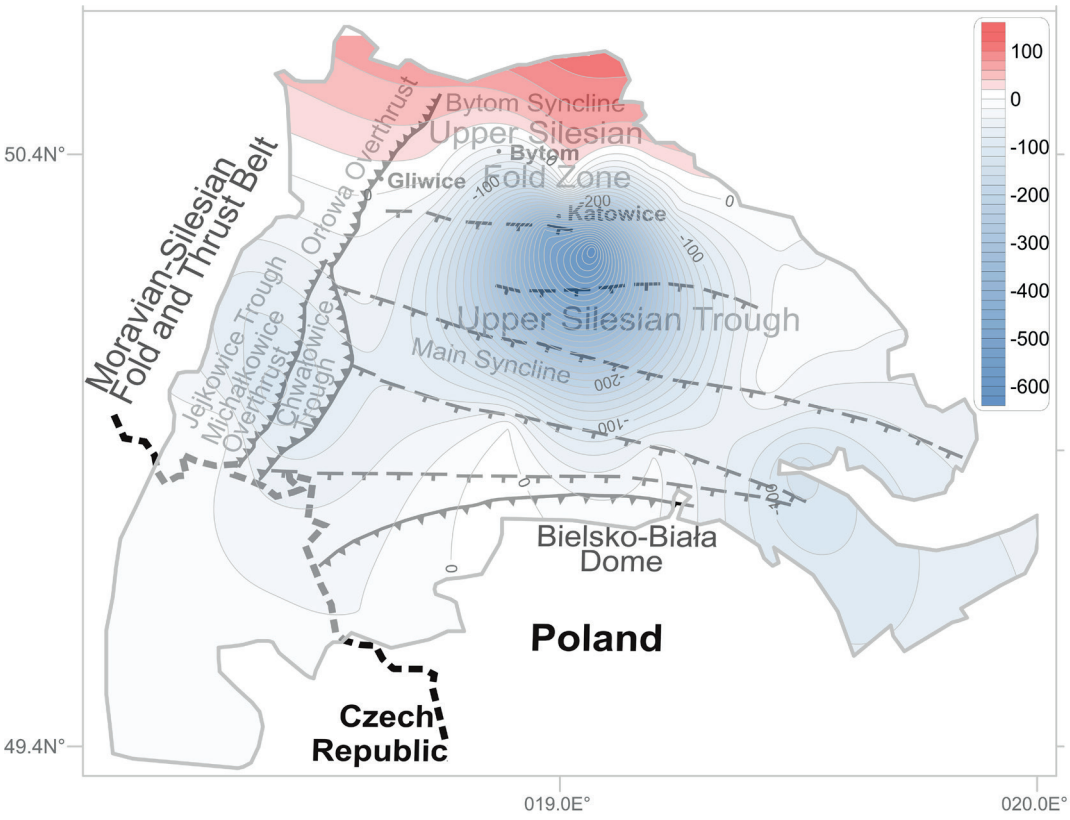

Fig. 6. *The distribution of the minimum horizontal extension in the area under study [nε]*

Another important parameter to be analysed is shear strain. It is the result of shear forces which push parts of the body in different directions and this is different to compression, which occurs when the two opposing forces are pushing into each other at the same point (i.e. they are not offset), resulting in compressive stress. So, it reflects the changes in stress regime, particularly in the direction of the forces acting in the deformation process. In the area of the USCB there are several triangles with large values of shear strain, showing large values of maximum and minimum horizontal extension: T11, T12, T6 and T21 (Fig. 7). Although rotation is a parameter within which the obtained values are rather small and which is characterized by high uncertainty values, their distribution is internally consistent and there is no apparent randomness.

In the triangles T6, T11, T12 and T21 the estimated values of rotation were found to be meaningful. Of all the triangles only the T11 demonstrates a clockwise rotation (Fig. 7). As has been shown, the central part of the USCB rotates in the opposite way to its surroundings and in general the clockwise rotation is demonstrated by the triangles located in the southern part of the area, and also in the western and the eastern (with some exceptions). Most of the northern triangles rotate in a counterclockwise direction. The most meaningful of the rotations are those found in the T11 and T12 triangles. They are neighbouring triangles and demonstrate high values of rotation and an opposite to each other direction of the rotation. This change of direction is observed in the north from them, but the rotation values of the triangles neighbouring T11 and T12 are smaller (Fig. 7).

The result of the distribution of the mentioned parameters reveals the characteristics of area strain. In our case only T12 and T11 demonstrated the noteworthy negative values of the parameter (respectively –525 and –128 nε), depicting a compressional regime which expresses a decrease of the area size (Fig. 8). There are as well zones demonstrating positive values of area strain. These are associated with an extensional regime which expresses the increase of an area size.

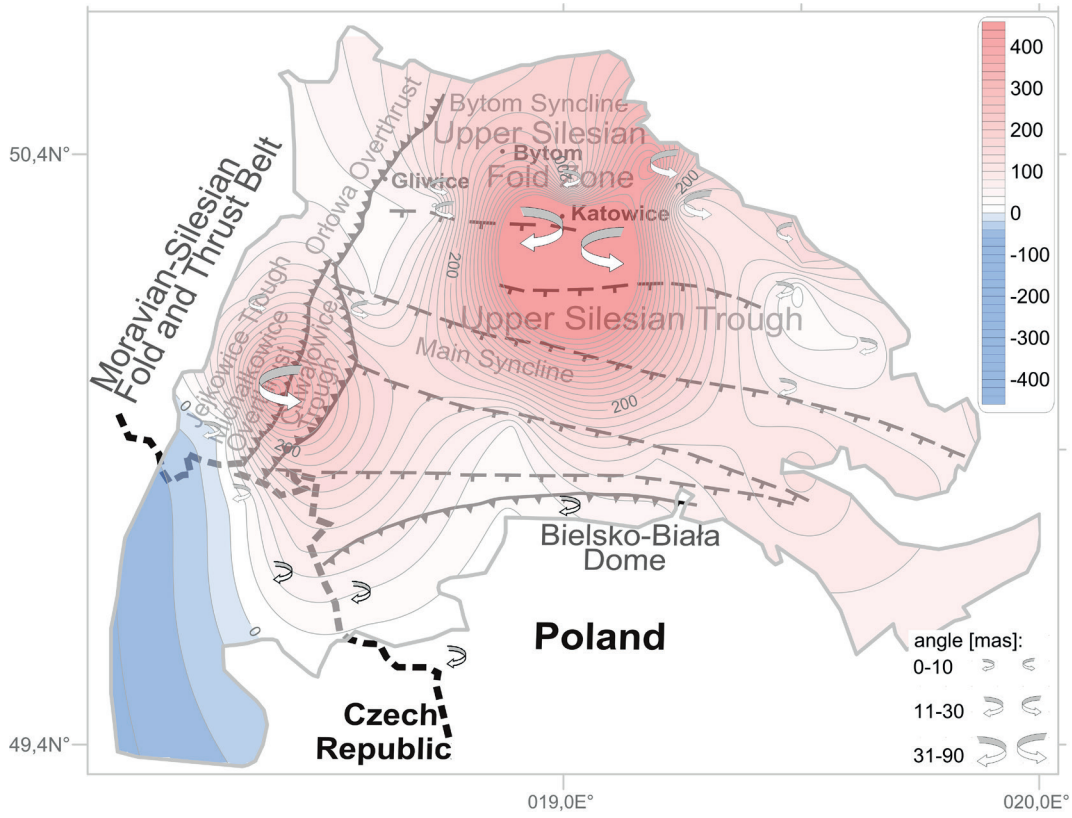

Fig. 7. *The Upper Silesian Coal Basin: the distribution of the maximum shear strain and rotations [nε]*

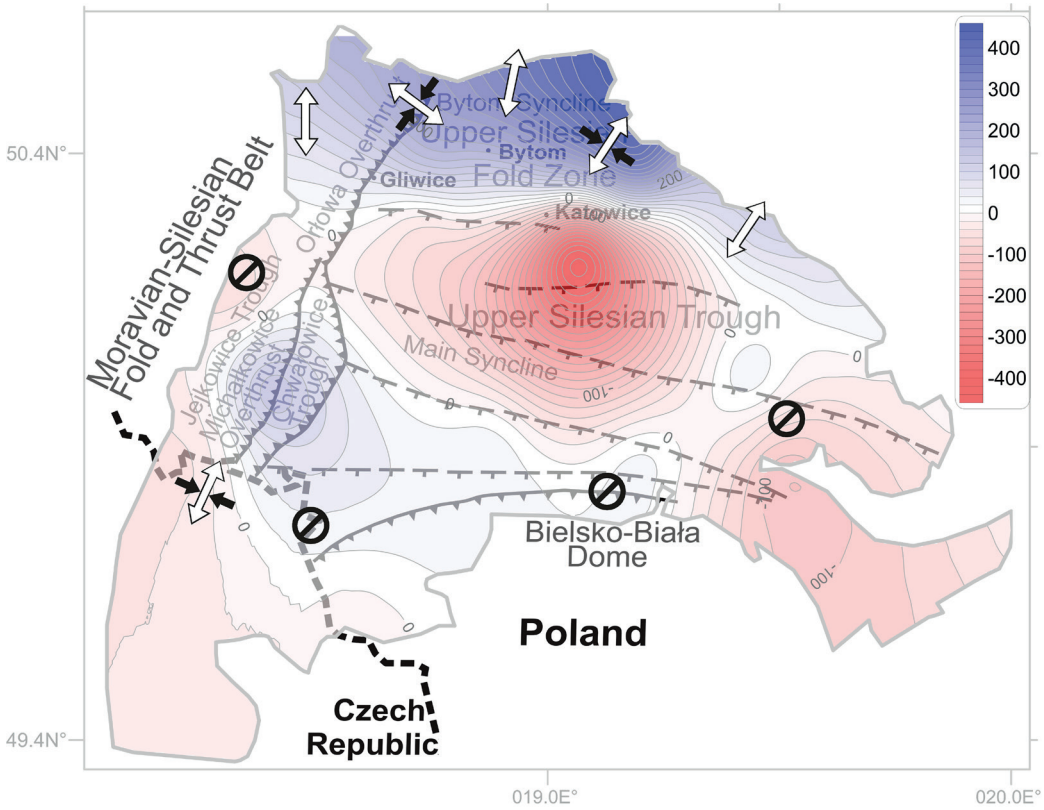

Fig. 8. *The Upper Silesian Coal Basin: the distribution of the area strain and strain regime [nε]*

Notable zones represented by the triangles for which the values of area strain exceed 100 nε occur mainly at the northern boundary and in the western part of the USCB (Fig. 8). So, it is the outlined area strain distribution which reflects all aforementioned spatial characteristics of the other strain parameters. This is an interesting feature: it is the positive value of the area strain which is evident in the total balance and which should be regarded as being the most distinctive attribute of the USCB area.

All of these detailed comments on the obtained results depicting the strain characteristics lead to some general remarks. Among them, the one of most fundamental importance is that there are two outstanding zones in the area of the USCB. One of them is located in the western part of the USCB and this zone represents an extensional regime with significant values of maximum horizontal extension and the azimuth of this parameter is NNE–SSW.

The other zone represents a large compression-extensional regime. It is covered by the triangles related to the stations TYCH, KATO and BEDZ. Although there are values of maximum horizontal extensions, minimum horizontal extensions are high and a compressional regime is definitely dominant there, seeing as how there is a change in the characteristics of the minimum extensions in the area of the BEDZ station and positive values of area strain occur (extensional regime). These subzones rotate in opposite directions. However, these are different characteristics when it comes to the area strain values or rotations, but taking into account the distribution of the maximum horizontal extensions value, there is no clear border. The third zone is related to the area of the OLKU stations. However, it is not revealed as clearly as the others but there is a significant increase of the maximum horizontal extensions of the SW–NE orientation and a clear extensional regime.

It is noteworthy that the centres of these three zones are almost collinear and the line containing them is SW–NE oriented.

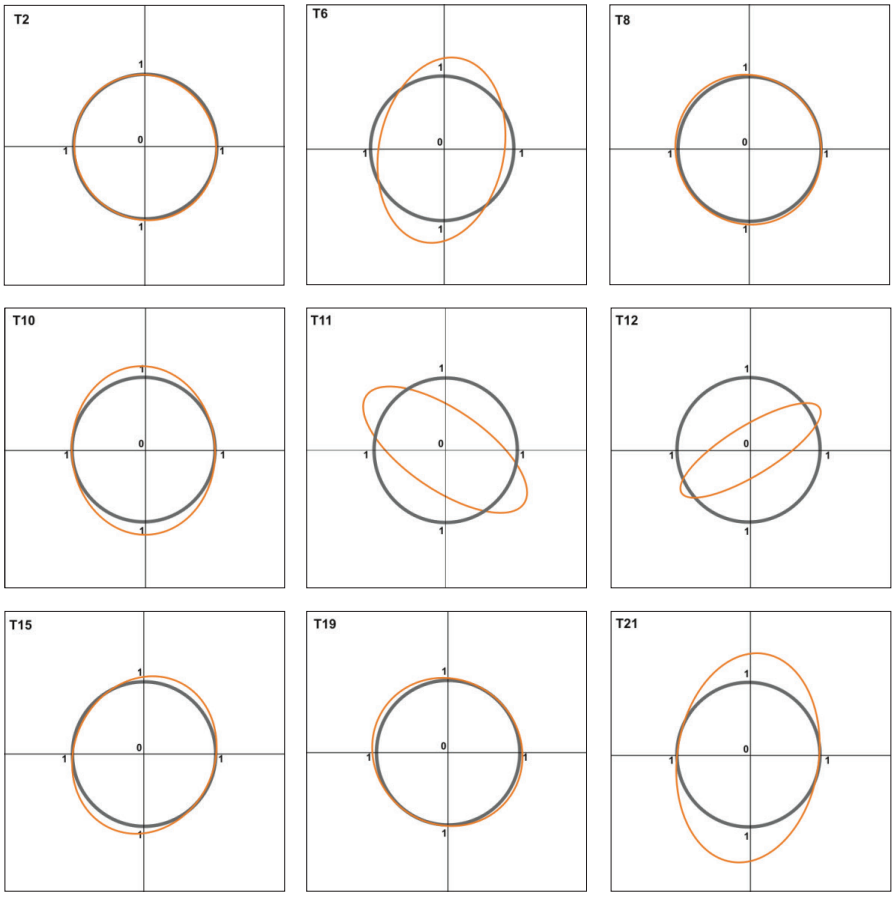

Fig. 9. *Strain ellipses determined for selected triangles which were analysed within this study*

Generalized characteristics of deformation in the USCB can be outlined by the strain ellipses, each of which describes the deformation of the corresponding triangle. Each of the selected ellipses can be regarded as being representative in their deformation characteristics for the part of the area under study (Fig. 9). Despite the fact that the distribution of the velocity vectors seems to be lacking any pattern to a large extent, as well as the fact that the uncertainty values of the strain ellipse parameters determined for some triangles amounted to high values, the distribution of the particular types of strain ellipses is completely non-accidental.

A clear pattern in the arrangement of the strain ellipses is visible at first sight: the eastern, the southern and the northwest parts of the area demonstrate no strains, whereas the western part shows both positive and negative extension and at the northern boundary of the area there are longitudinally oriented extensions. These extensions are transformed into positive and negative values with a SE–NW orientation of the maximum extensions. They again are transformed at the longitudinal axe of the area into longitudinally oriented extensions, and then are again transformed into positive and negative extensions but with a SW–NE orientation of the maximum extension. All of this finally leads to a SW–NE orientated extension at the NE part of the area.

This distribution suggests the northward displacement of the region with a change in the stress regime in the central part of the USCB. This is a zone where the orientation of the rotation is changed as the orientation of elongations of the strain ellipses.

CONCLUSIONS

The USCB is one of the most tectonically complicated Palaeozoic molasse basins of the European Variscides, being characterized by a zonal tectonic pattern that includes both complicated thrust-fold

deformations and relatively simpler normal fault and transtensional tectonics (Dopita & Kumpera 1993, Grygar & Wacławik 2011). Geodetic satellite data from a moderately dense network enable the application of triangulation to construct several dozen different triangles for strain analysis, where all the deformation parameters were calculated for different triangle centroids. No matter how small the displacement rates of the stations, a strong variation in deformation parameters is noticeable. Strain characteristics show that the deformation parameters in the region are unusual, such that the area is not homogeneously deformed. A more detailed analysis also enables the identification of several separate zones in which, in contrast, strain characteristics are homogeneous, the most important of which are maximum and minimum horizontal extension, maximum shear, and the area strain. Further, compression and extension, which dominate in the USCB area, occur in particular zones: in general compression occurs in the central part of the area and extension occurs in the western and northern parts and in part of the eastern area. In general, the central part undergoing compression (the Upper Silesian Trough) is surrounded by extensional zones. Such spatial characteristics of strain suggest compressional collapse of the UST and inward compression to produce extension in the outer parts. The lack of extension in the southern part of the area could indicate a tectonic push from a southerly direction. It seems that the distributions of the determined strain parameters reveal a discontinuous nature of surface deformations and that strain zones are probably separated by tectonic discontinuities. Strain distribution follows a zonal tectonic pattern within the USCB: a block zone of compression, a folded zone with extension, and a fold and block zone with extension, all of these zones suggesting the impact of networks of interconnected faults separating quasi-rigid blocks.

There are two main regions characterized by high levels of seismic activity (Fig. 3C):

1) the Jejkowice and Chwałowice troughs;
2) Bytom Trough, Upper Silesian Fold Zone and Upper Silesian Trough – particularlythe area at the contact of these units.

Both regions are characterized by the highest values of: maximal horizontal strain, rotations and area strain. However, there are some differences. As mentioned earlier, only the Upper Silesian Trough area is subject to compression, whereas the other region shows extensional deformations. There seems to be an interconnectedness between the tectonic setting of the area, the geokinematics and the tectonic strain fields in the USCB area, and also a connection with the mining activity operating in unsustainable geomechanical conditions. Their combination produces a result which is a phenomenon of the seismicity in the USCB. Tectonics is the basic factor and the one which determines the formation of high-energy seismic tremors.

One should perceive the slow accumulation of stresses, and the formation of seismogenic structures (especially in faulted zones), which has led to precipitous releases of seismic energy triggered by mining operations.

The research results on the strain characteristics in the USCB which are presented here indicate the fundamental (primary) source of this phenomenon. Although the general results are unambiguous, a strict quantitative approach to the strain parameters in some cases should be handled with a certain degree of caution. It may be seen, for example, that the obtained values of the strain parameters should be regarded as rough estimates which reflect the compressional-extensional setting of the USCB area and should be clarified by more intensive future research. It requires specially designed micro-networks or at least an increase in the number of stations, especially in the areas of the USCB where they are absent (mainly in the southern part).

Taking into account some limitations of the GNSS technique, the results presented here should be regarded being as evidence. There are however some undeniable facts, as for example the presence of a general pattern of strain in the USCB. These facts and insights may benefit researchers from other disciplines engaged in the geological and geophysical analysis of the USCB area.

I would like to extend my special thanks to the Head Office of Geodesy and Cartography in Poland for making the postprocessed data available i.e. the ETRF coordinates of the analysed stations. We wish to thank the Nevada Geodetic Laboratory,

UNAVCO and European-Mediterranean Seismological Centre for making the data used herein freely available.

I would like to thank the authors of the works devoted to the detailed and extensive descriptions of the algorithm that was used in this work, and above all, R. W. Allmendinger, N. Cardozo, D. M. Fisher and V. Cronin. I dedicate the publication of this paper to all the authors I cite and with whom I have had contact during the years of my academic education, so with this work I express my thanks to all these tutors: W. M. Zuberek, L. Teper, D. Jura, A. F. Idziak, G. Sagan, J. Żaba, and B. Żogała.

REFERENCES

Aleksandrowicz S.W., 1964. Przejawy tektoniki mioceńskiej w Zagłębiu Górnośląskim [Miocene tectonics in the Upper Silesian Basin]. *Acta Geologica Polonica*, 14(2), 175–228.

Allmendinger R.W., Reilinger R. & Loveless J.P., 2007. Strain and rotation rate from GPS in Tibet, Anatolia, and the Altiplano. *Tectonics*, 26(2), TC3013. https://doi.org/10.1029/2006TC002030.

Allmendinger R.W., Loveless J.P., Pritchard M.E. & Meade B., 2009. From decades to epochs: Spanning the gap between geodesy and structural geology of active mountain belts. *Journal of Structural Geology*, 31(11), 1409–1422. https://doi.org/10.1016/j.jsg.2009.08.008.

Allmendinger R.W., Cardozo N. & Fisher D., 2012. *Structural Geology Algorithms: Vectors and Tensor*s. Cambridge University Press, Cambridge.

Araszkiewicz A., Figurski M. & Jarosiński M., 2016. Erroneous GNSS strain rate patterns and their application to investigate the tectonic credibility of GNSS velocities. *Acta Geophysica*, 64(5), 1412–1429. https://doi.org/10.1515/acgeo-2016-0057.

Argus D.F., Heflin M.B., Peltzer G., Crampe F. & Webb F.H., 2005. Interseismic strain accumulation and anthropogenic motion in metropolitan Los Angeles. *Journal of Geophysical Research*, 110(B4), B04401, 1–26. https://doi.org/10.1029/2003JB002934.

Avouac J.P. & Tapponnier P., 1993. Kinematic model of active deformation in central Asia. *Geophysical Research Letters*, 20(10), 895–898. https://doi.org/10.1029/93GL0012.

Bawden G.W., Thatcher W., Stein R.S., Hudnut K.W. & Peltzer G., 2001. Tectonic contraction across Los Angeles after removal of groundwater pumping effects. *Nature*, 412, 812–815. https://doi.org/10.1038/35090558.

Blewitt G., Lavallée D., Clarke P. & Nurutdinov K., 2001. A new global mode of earth deformation: Seasonal cycle detected. *Science*, 294(5550), 2342–2345. https://doi.org/10.1126/science.1065328.

Blewitt G., Hammond W.C. & Kreemer C., 2018. Harnessing the GPS data explosion for interdisciplinary science. *Eos*, 99, 18–22. https://doi.org/10.1029/2018EO104623.

Bogusz J., Kłos A., Figurski M., Jarosiński M. & Kontny B., 2013. Investigation of the reliability of local strain analysis by means of the triangle modelling. *Acta Geodynamica et Geomaterialia*, 10(3), 93–305. https://doi.org/10.13168/AGG.2013.0029.

Bosy J., Graszka W. & Leończyk M., 2007. ASG-EUPOS – a multifunctional precise satellite positioning system in Poland. *TransNav, International Journal on Marine Navigation and Safety of Sea Transportation*, 1(4), 371–374.

Botor D., Dunkl I., Anczkiewicz A. & Mazur S., 2017. Post-Variscan thermal history of the Moravo-Silesian lower Carboniferous Culm Basin (NE Czech Republic – SW Poland). *Tectonophysics*, 712–713, 643–662. https://doi.org/10.1016/j.tecto.2017.06.035.

Buła Z. & Kotas A. (red.), 1994. *Atlas geologiczny Górnośląskiego Zagłębia Węglowego: 1:100 000. Cz. 3, Mapy geologiczno-strukturalne* [*Geological atlas of the Upper Silesian Coal Basin. P. 3, Structural geological maps*]. Państwowy Instytut Geologiczny, Warszawa.

Buła Z., Żaba J. & Habryn R., 2008. Regionalizacja tektoniczna Polski – Polska południowa (blok górnośląski i blok małopolski) [Tectonic subdivision of Poland: Southern Poland (Upper Silesian Block and Małopolska Block)]. *Przegląd Geologiczny*, 56(10), 912–920. https://geojournals.pgi.gov.pl/pg/article/view/30756/23445.

Cronin V., Olds S., Pratt-Sitaula B., Resor P., West N., Hammond W.C., Kreemer C., 2012. *Infinitesimal strain analysis using GPS data: Module for structural geology or geophysics course*. UNAVCO, Geodetic Education Resources. https://serc.carleton.edu/getsi/teaching_materials/gps_strain/unit4.html [access: 1.09.2024].

Doktorowicz-Hrebnicki S., 1963. Zależność między ruchami dna basenu sedymentacyjnego karbonu górnego a późniejszą jego tektoniką [Interdependence of the movements of the floor of the Upper Carboniferous sedimentation basin and its later tectonics]. *Prace Instytutu Geologicznego*, 30(4), 263–276.

Dopita M. & Kumpera O., 1993. Geology of the Ostrava-Karviná coalfield, Upper Silesian Basin, Czech Republic, and its influence on mining. *International Journal of Coal Geology*, 23(1–4), 291–321. https://doi.org/10.1016/0166-5162(93)90053-D.

Dubiński J., Stec K. & Bukowska M., 2019. Geomechanical and tectonophysical conditions of mining-induced seismicity in the Upper Silesian Coal Basin in Poland: A case study. *Archives of Mining Sciences*, 64(1), 163–180. https://doi.org/10.24425/ams.2019.126278.

Dyjor S., Dendewicz A., Grodzicki A., Sadowska A., 1978. Neogeńska i staroplejstońska sedymentacja w obrębie stref zapadliskowych rowów Paczkowa i Kędzierzyna [The Neogene and old-Pleistocene sedimentation in the Paczków and Kędzierzyn graben zones]. *Geologia Sudetica*, 13(1), 7–139. https://geojournals.pgi.gov.pl/gs/article/view/25392.

JCGM, 2008. *Evaluation of measurement data – Guide to the expression of uncertainty in measurement = Évaluation des données de mesure – Guide pour l'expression de l'incertitude de mesure* (JCGM 100:2008). Joint Committee for Guides in Metrology, Sèvres. https://www.bipm.org/utils/common/documents/jcgm/JCGM_100_2008_E.pdf [access: 1.09.2024].

Gibowicz S.J., 1990. Seismicity induced by mining. *Advances in Geophysics*, 32, 1–74. https://doi.org/10.1016/S0065-2687(08)60426-4.

Goszcz A., 1985. Kompakcja tektoniczna jako przyczyna naturalnej skłonności skał do wstrząsów górniczych i tąpań. *Przegląd Górniczy*, 7–8, 239–244.

Goszcz A., 1986. Tektonofizyczne przyczyny występowania wstrząsów górniczych [Tectonophysical origin of mining tremors]. [in:] *Wybrane zagadnienia geofizycznych badań w kopalniach: Jastarnia, 6–10 V 1985 = Some geophysical problems in mine*, Publications of the Institute of Geophysics Polish Academy of Sciences, M-8(191), Państwowe Wydawnictwo, Warszawa – Łódź, 61–75.

Goszcz A., 1999. *Elementy mechaniki skał oraz tąpania w polskich kopalniach węgla i miedzi*. Biblioteka Szkoły Eksploatacji Podziemnej. Seria z Lampką Górniczą, nr 2, Wydawnictwo Instytutu Gospodarki Surowcami Mineralnymi i Energią PAN, Kraków.

Grygar R. & Wacławik P., 2011. Structural-tectonic conditions of Karviná Subbasin with regard to its position in the apical zone of Variscan accretion wedge. *Acta Montanistica Slovaca*, 16(2), 159–175.

Heki K., 2001. Seasonal modulation of interseismic strain buildup in northeastern Japan driven by snow loads. *Science*, 293(5527), 89–92. https://doi.org/10.1126/science.1061056.

Herbich E., 1981. Analiza tektoniczna sieci uskokowej Górnośląskiego Zagłębia Węglowego [A tectonic analysis of the fault network of the Upper Silesia Coal Basin]. *Annales Societatis Geologorum Poloniae*, 51(3–4), 383–434. http://www.asgp.pl/sites/default/files/volumes/51_3-4_383_434.pdf [access: 1.09.2024].

Idziak A.F., Teper L. & Zuberek W.M., 1999. *Sejsmiczność a tektonika Górnośląskiego Zagłębia Węglowego* [*Seismic activity and tectonics of the Upper Silesian Coal Basin*]. Prace Naukowe Uniwersytetu Śląskiego w Katowicach, 1793, Wydawnictwo Uniwersytetu Śląskiego, Katowice. https://core.ac.uk/download/pdf/270093587.pdf [access: 1.09.2024].

Jarosiński M., 1998. Contemporary stress field distortion in the Polish part of the Western Outer Carpathians and their basement. *Tectonophysics*, 297(1–4), 91–119. https://doi.org/10.1016/S0040-1951(98)00165-6.

Jarosiński M., 2005. Ongoing tectonic reactivation of the Outer Carpathians and its impact on the foreland: Results of borehole breakout measurements in Poland. *Tectonophysics*, 410(1–4), 189–216. https://doi.org/10.1016/j.tecto.2004.12.040.

Jarosiński M., 2006. Recent tectonic stress field investigations in Poland: A state of the art. *Geological Quarterly*, 50(3), 303–321.

Jarosinski M., Beekman F., Matenco L. & Cloetingh S., 2011. Mechanics of basin inversion: Finite element modelling of the Pannonian Basin System. *Tectonophysics*, 502(1–2), 121–145. https://doi.org/10.1016/j.tecto.2009.09.015.

Jura D., 1995. The young-Alpine morphotectonics of the Silesian Carpathian Foredeep and the recent geodynamics of the Upper Silesian Coal Basin. *Technika Poszukiwań Geologicznych: Geosynoptyka i Geotermia*, 38(1), 9–11.

Jura D., 1999. Young Alpine Klonica Fault scarps of the metacarpathian in the Silesian Upland. *Technika Poszukiwań Geologicznych: Geosynoptyka i Geotermia*, 38(1), 52–56.

Jura D., 2001. *Morfotektonika i ewolucja różnowiekowej niezgodności w stropie utworów karbonu Górnośląskiego Zagłębia Węglowego* [*Morphotectonics and evolution of discordances of different age present in the top surface of the Carboniferous of the Upper Silesia Coal Basin*]. Prace Naukowe Uniwersytetu Śląskiego, 1952, Wydawnictwo Uniwersytetu Śląskiego, Katowice.

Jureczka J. & Kotas A., 1995. Coal deposits – Upper Silesian Coal Basin. [in:] Zdanowski A. & Żakowa H. (eds.), *The Carboniferous System in Poland*, Prace Państwowego Instytutu Geologicznego, 148, Państwowy Instytut Geologiczny, Warszawa, 164–173.

Kotas A., 1985. Uwagi o ewolucji strukturalnej Górnośląskiego Zagłębia Węglowego. [in:] Trzepierczyński J. (red.), *Tektonika Górnośląskiego Zagłębia Węglowego: Sosnowiec 1985, maj 31 – czerwiec 1*, Uniwersytet Śląski, Sosnowiec, 17–46.

Kotas A., 1995. Upper Silesian Coal Basin: Lithostratigraphy, sedimentology, and paleogeographic development. [in:] Zdanowski A. & Żakowa H. (eds.), *The Carboniferous System in Poland*, Prace Państwowego Instytutu Geologicznego, 148, Państwowy Instytut Geologiczny, Warszawa, 124–135.

Kotlicka G.N., 1981. Neotektonika doliny Górnej Odry [The neotectonics of the valley of the Upper Odra]. *Z Badań Czwartorzędu w Polsce*, 23, *Biuletyn Instytutu Geologicznego*, 321, 165–175.

Krawczyk A. & Grzybek R., 2018. An evaluation of processing InSAR Sentinel-1A/B data for correlation of mining subsidence with mining induced tremors in the Upper Silesian Coal Basin (Poland). *E3S Web Conference*, 26, 00003. https://doi.org/10.1051/e3sconf/20182600003.

Kroner U., Mansy J.-L., Mazur S., Aleksandrowski P., Hann H.P., Huckriede H., Lacquement F., Lamarche J., Ledru P., Pharaoh T.C., Zedler H., Zeh A. & Zulauf G., 2008. Variscan tectonics. [in:] McCann T. (ed.), *The geology of Central Europe. Volume 1: Precambrian and Palaeozoic*, Geological Society, London, 599–664. https://doi.org/10.1144/CEV1P.11.

Kusiak M., Kędzior A., Paszkowski M., Suzuki K., Gonzalez-Alvarez I., Wajsprych B. & Doktor M., 2006. Provenance implications of Th-U-Pb electron microprobe ages from detrital monazite in the Carboniferous Upper Silesia Coal Basin, Poland. *Lithos*, 88(1–4), 56–71. https://doi.org/10.1016/j.lithos.2005.08.004.

Lazos I., Stergiou C.L., Chatzipetros A., Pikridas C., Bitharis S. & Melfos V., 2018. Active tectonics (extensional regime and rotations) and Tertiary mineralization occurrences within Central Macedonia, Greece. [in:] Koukousioura O. & Chatzipetros A. (eds.), *The 9th International INQUA Meeting on Paleoseismology, Active Tectonics and Archeoseismology (PATA), 25 – 27 June 2018, Possidi, Greece*, School of Geology of the Aristotle University of Thessaloniki, Thessaloniki, 145–148.

Lazos I., Pikridas C., Chatzipetros A. & Pavlides S., 2020. Determination of local active tectonics regime in central and northern Greece, using primary geodetic data. *Applied Geomatics*, 13(1), 3–17. https://doi.org/10.1007/s12518-020-00310-x.

Lewandowski J., 1995. Neotectonic structures in the Racibórz-Oświęcim Basin, Upper Silesia, Southern Poland. *Folia Quaternaria*, 66, 99–104.

Lewandowski J., 2007. Neotectonic structures of the Upper Silesian region, Southern Poland. *Studia Quaternaria*, 24, 21–28.

Mendecki M., Szczygieł J., Lizurek G. & Teper L., 2020. Mining-triggered seismicity governed by a fold hinge zone: The Upper Silesian Coal Basin, Poland. *Engineering Geology*, 274, 105728. https://doi.org/10.1016/j.enggeo.2020.105728.

Michel V. & Person T., 2003. From geodetic monitoring to deformation tensors and their reliability. [in:] Stiros S.C. & Pytharouli S. (eds.), *Proceedings 11th International FIG Symposium on Deformation Measurements: Santorini (Thera) Island, Greece, 25–28 May 2003*, Patras University, Patras, 463–469.

Overacker J., Hammond W.C., Blewitt G. & Kreemer C., 2022. Vertical land motion of the High Plains aquifer region of the United States: Effect of aquifer confinement style, climate variability, and anthropogenic activity. *Water Resources Research*, 58, e2021WR031635. https://doi.org/10.1029/2021WR031635.

Patyńska R. & Stec K., 2017. Regional rockburst indicator for structural units of Upper Silesia Coal Basin. *Studia Geotechnica et Mechanica*, 39(3), 27–37. https://doi.org/10.1515/sgem-2017-0027.

Pospíšil L., Otava J. & Hudečková E., 2019. Utilization of archive geophysical data for geodynamical studies in the Sudetes: Example of Bělá fault zone (The Nízký Jeseník Mts). *Acta Geodynamica et Geomaterialia*, 16(195), 281–291. https://doi.org/10.13168/AGG.2019.0024.

Ptáček J., Grygar R., Koníček P. & Waclawik P., 2012. The impact of Outer Western Carpathian nappe tectonics on the recent stress-strain state in the Upper Silesian Coal Basin (Moravosilesian Zone, Bohemian Massif). *Geologica Carpathica*, 63(1), 3–11. https://doi.org/10.2478/v10096-012-0002-x.

Roštínský P., Pospíšil L., Švábenský O., Kašing M. & Nováková E., 2020. Risk faults in stable crust of the eastern Bohemian Massif identified by integrating GNSS, levelling, geological, geomorphological and geophysical data. *Tectonophysics*, 785, 228427. https://doi.org/10.1016/j.tecto.2020.228427.

Roštínský P., Pospíšil L., Švábenský O., Melnyk A. & Nováková E., 2024. Recent reactivation of Variscan tectonic zones: A case of Rodl–Kaplice–Blanice fault system (Bohemian Massif, Austria/Czech Republic). *Surveys in Geophysics*, 45(3), 609–661. https://doi.org/10.1007/s10712-023-09811-x.

Schenková Z., Kottnauer P., Schenk V., Cajthamlová-Grácová M., Mantlík F. & Kujal R., 2009. Investigation of the recent crustal movements of the eastern part of the Bohemian Massif using GPS technology. *Acta Research Reports*, 18, 17–25.

Schmidt D.A. & Bürgmann R., 2003. Time-dependent land uplift and subsidence in the Santa Clara Valley, California, from a large interferometric synthetic aperture radar data set. *Journal of Geophysical Research*, 108(B9), 2416. https://doi.org/10.1029/2002JB002267.

Segall P. & Davis J.L., 1997. GPS applications for geodynamics and earthquake studies. *Annual Review of Earth and Planetary Sciences*, 25(1), 301–336. https://doi.org/10.1146/annurev.earth.25.1.301.

Sigbjörnsson R., Snæbjörnsson J., Valsson G., Sigurdsson T. & Rupakhety R., 2018. Surface strain rate tensor field for Iceland based on a GPS network. [in:] Rupakhety R. & Ólafsson S. (eds.), *Earthquake Engineering and Structural Dynamics in Memory of Ragnar Sigbjörnsson. ICESD 2017*, Geotechnical, Geological and Earthquake Engineering, 44, Springer, Cham, 107–119. https://doi.org/10.1007/978-3-319-62099-2_9.

Szczerbowski Z., 2019. Czasoprzestrzenne związki pomiędzy sezonowymi zmianami pozycji stacji GNSS a wysokoenergetycznymi wstrząsami sejsmicznymi w Górnośląskim Zagłębiu Węglowym [Spatiotemporal relations between seasonal changes of positions of GNSS stations and high energy tremors in The Upper Silesian Coal Basin]. *Przegląd Górniczy*, 75(12), 30–37.

Szczerbowski Z. & Jura J., 2015. Mining induced seismic events and surface deformations monitored by GPS permanent stations. *Acta Geodynamica et Geomaterialia*, 12(3), 237–248. https://doi.org/10.13168/AGG.2015.0023.

Teper L., 1998. *Wpływ nieciągłości podłoża karbonu na sejsmotektonikę północnej części Górnośląskiego Zagłębia Węglowego* [*Seismotectonics in the Northern Part of the Upper Silesian Coal Basin: Deep-seated Fractures-Controlled Pattern*]. Prace Naukowe Uniwersytetu Śląskiego w Katowicach, 1715, Wydawnictwo Uniwersytetu Śląskiego, Katowice.

Teper L. & Sagan G., 1995. Geological history and mining seismicity in Upper Silesia (Poland). [in:] Rossmanith H.P. (ed.), *Mechanics of Jointed and Faulted Rock*, Balkema, Rotterdam, 939–943.

Teper L., Idziak A.F., Sagan G. & Zuberek W.M., 1992. New approach to the studies of the relations between tectonics and mining tremors occurrence on example of Upper Silesian Coal Basin (Poland). *Acta Montana A*, 2(88), 161–177.

Teisseyre R., 1983. Indukowana sejsmiczność i wstrząsy pochodzenia eksploatacyjnego. [in:] Jucha S. & Teisseyre R. (red.), *Fizyka i ewolucja wnętrza Ziemi. Część 2*, Państwowe Wydawnictwo Naukowe, Warszawa, 254–260.

Witkowski W.T., Łukosz M., Guzy A. & Hejmanowski R., 2021. Estimation of mining-induced horizontal strain tensor of land surface applying InSAR. *Minerals*, 11(7), 788. https://doi.org/10.3390/min11070788.

Znosko J., 1965. Pozycja tektoniczna śląsko-krakowskiego zagłębia węglowego [Tectonic position of the Silesia-Cracow Coal Basin]. *Z Badań Tektonicznych w Polsce*, 1, *Biuletyn Instytutu Geologicznego*, 188, s. 73–120.

Zuberek W.M., Teper L., Idziak A.F. & Sagan G., 1996. Tectonophysical approach to the description of mining induced seismicity in the Upper Silesia. [in:] Idziak A. (ed.), *Tectonophysics of Mining Areas*, Prace Naukowe Uniwersytetu Śląskiego w Katowicach, 1602, Wydawnictwo Uniwersytetu Śląskiego, Katowice, 79–98.

Zuberek W.M., Teper L., Idziak A.F. & Sagan G., 1997. Seismicity and tectonics in the Upper Silesian Coal Basin, Poland. [in:] Podemski M. (ed.), *Proceedings of the XIII International Congress on the Carboniferous and Permian*, Prace Państwowego Instytutu Geologicznego, 157, Państwowy Instytut Geologiczny, Warszawa, 199–207.

Zuchiewicz W., Badura J. & Jarosiński M., 2007. Neotectonics of Poland: An overview of active faulting. *Studia Quaternaria*, 24, 5–20.

Żelaźniewicz A., Aleksandrowski P., Buła Z., Karnkowski P., Konon A., Ślęczka A., Żaba J. & Żytko K., 2011. *Regionalizacja tektoniczna Polski*. Komitet Nauk Geologicznych PAN, Wrocław.